

PCCP

Accepted Manuscript



This is an *Accepted Manuscript*, which has been through the Royal Society of Chemistry peer review process and has been accepted for publication.

Accepted Manuscripts are published online shortly after acceptance, before technical editing, formatting and proof reading. Using this free service, authors can make their results available to the community, in citable form, before we publish the edited article. We will replace this *Accepted Manuscript* with the edited and formatted *Advance Article* as soon as it is available.

You can find more information about *Accepted Manuscripts* in the [Information for Authors](#).

Please note that technical editing may introduce minor changes to the text and/or graphics, which may alter content. The journal's standard [Terms & Conditions](#) and the [Ethical guidelines](#) still apply. In no event shall the Royal Society of Chemistry be held responsible for any errors or omissions in this *Accepted Manuscript* or any consequences arising from the use of any information it contains.

Cite this: DOI: 10.1039/c0xx00000x

www.rsc.org/xxxxxx

ARTICLE TYPE

Origin of high activity but low CO₂ selectivity on binary PtSn in the direct ethanol fuel cell†

Jia-Mei Jin,^a Tian Sheng,^a Xiao Lin,^a Richard Kavanagh,^a Philip Hamer,^a Peijun Hu,^a Christopher Hardacre,^{*a} Alex Martinez-Bonastre,^b Jonathan Sharman,^b David Thompsett^b and Wen-Feng Lin^{*a}

5 Received (in XXX, XXX) Xth XXXXXXXXXX 20XX, Accepted Xth XXXXXXXXXX 20XX

DOI: 10.1039/b000000x

The most active binary PtSn catalyst for direct ethanol fuel cell applications has been studied at 20 °C and 60 °C, using variable temperature electrochemical *in-situ* FTIR. In comparison with Pt, binary PtSn inhibits ethanol dissociation to CO(a), but promotes partial oxidation to acetaldehyde and acetic acid. Increasing the temperature from 20 °C to 60 °C facilitates both ethanol dissociation to CO(a) and then further oxidation to CO₂, leading to an increased selectivity towards CO₂; however, acetaldehyde and acetic acid are still the main products. Potential-dependent phase diagrams for surface oxidants of OH(a) formation on Pt(111), Pt(211) and Sn modified Pt(111) and Pt(211) surfaces have been determined using density functional theory (DFT) calculations. It is shown that Sn promotes the formation of OH(a) with a lower onset potential on the Pt(111) surface, whereas an increase in the onset potential is found on modification of the (211) surface. In addition, Sn inhibits the Pt(211) step edge with respect to ethanol C-C bond breaking compared with that found on the pure Pt, which reduces the formation of CO(a). Sn was also found to facilitate ethanol dehydrogenation and partial oxidation to acetaldehyde and acetic acid which, combined with the more facile OH(a) formation on the Pt(111) surface, gives us a clear understanding of the experimentally determined results. This combined electrochemical *in-situ* FTIR and DFT study, provides, for the first time, an insight into the long-term puzzling features of the high activity but low CO₂ production found on binary PtSn ethanol fuel cell catalysts.

1 Introduction

The increasing environmental concerns and the limited resources of fossil fuels have stimulated an intensive search for clean and sustainable energy sources. Fuel cells are a promising new clean energy technology due to their potential high energy efficiency and low emissions. Among many important applications of fuel cells, low temperature Direct Alcohol Fuel Cells (DAFCs) are extremely attractive as power sources for transportation, mobile and portable applications.^{1,2} Compared with hydrogen-fed fuel cells, which need to employ reforming technology and/or require hydrogen storage, DAFCs use a simple liquid fuel. Methanol is a promising fuel because it is the most easily oxidized alcohol and thus the direct methanol fuel cell (DMFC) has been developed as the first generation technology for the portable power market.^{3,4} Nevertheless, there are significant problems with methanol for example, methanol is more toxic and has lower energy density than ethanol (6.1 vs. 8.0 kWh kg⁻¹). Therefore, carbon-neutral bio-ethanol is an attractive future proposition. However, the implementation of ethanol fuel cell technology has been hindered by the low rates for the ethanol oxidation reaction (EOR) at the anode.⁵⁻⁸ As a result, the most critical challenge for the use of ethanol in direct ethanol fuel cells (DEFC) is to find an efficient electrocatalyst for EOR, in terms of both activity (high activity at

low over-potential) and CO₂ selectivity in order to achieve the maximum 12 e⁻ per ethanol molecule.

In general, it has been shown that pure Pt systems are not efficient catalysts for EOR and thus modification of Pt electrode with other metals including Ru, Rh, Ir, Sn and Sb has been investigated extensively.⁶⁻²¹ To date, electrodes based on Pt and Sn have been identified catalysts which exhibit the highest activity for the EOR,⁶⁻¹⁸ albeit with a low selectivity to CO₂. It is interesting to point out that Vigier et al. initially reported a higher selectivity to CO₂ observed on PtSn than that on pure Pt;⁹ however, the same group reported later that PtSn actually decreases the CO₂ selectivity compared to pure Pt,^{10,11} which was confirmed by all other reports.¹²⁻¹⁸ Despite extensive research in determining the structure, reactivity and selectivity of PtSn catalysts, the fundamental understanding of the mechanisms which govern the promotional effect of Sn is still lacking. In particular, the processes which facilitate the initial stages of ethanol adsorption/dissociation and oxidation at lower potentials compared with many other systems. Herein, we have examined the reaction mechanism of the EOR over Pt and PtSn surfaces and provided a fundamental understanding of the Sn promotion of the Pt at the molecular and electronic levels, for the first time, using electrochemistry combined with *in-situ* FTIR spectroscopy and density functional theory (DFT) calculations. It is also worth pointing out that although classical

electrochemical current/voltage/time techniques are highly sensitive and able to provide a wealth of kinetic data, they lack the ability to provide essential molecular information. Major breakthroughs in the understanding of the mechanism at the electrode/electrolyte interface were triggered in particular by the development, at the beginning of the 1980s, of *in-situ* electrochemical infrared (IR) techniques. Since then, many *in-situ* IR studies have been reported, generally using *in-situ* Fourier Transform infrared (FTIR) spectroscopy and elucidating the role of key adsorbates, such as CO(a) or other carbonaceous fragments in electro-catalytically relevant reactions. Adsorbed CO can be detected on electrodes down to a few percentages of a monolayer with FTIR, and the positions and intensities of the vibrational bands of the various adsorbed CO species provide information about the adlayer structure and interfacial environment. The overwhelming majority of *in-situ* FTIR spectroelectrochemical measurements to date have been carried out at room temperature, due to the fact that effective control of the temperature of an *in-situ* electrochemical spectroscopic system is not straightforward. Nevertheless, we have successfully developed a sophisticated variable temperature *in-situ* FTIR system^{22,23} and observed a significant effect of temperature on surface electrochemistry. In this study, the results at room temperature have been compared with the activity and selectivity at 60 °C which is more relevant to practical DEFC operation.

2 Experimental section

2.1 Experimental methods

The electrochemical *in situ* FTIR spectroscopy system consists of a Varian 670-IR air-bearing FTIR spectrometer equipped with a Duraglow infrared source and a narrow-band MCT detector, an Autolab PGSTAT302N potentiostat, a home built reflectance optical bench comprising of four reflective mirrors and a home-built variable temperature spectro-electrochemical cell fitted with a hemispherical CaF₂ window (Medway Optics Ltd).^{22,23} The cell was vertically mounted on the lid of the sample compartment of the FTIR spectrometer and was designed to allow electrolyte exchange under potential control. The cell was jacketed to allow careful control of the temperature of the electrolyte in the body of the cell. To ensure that this control extended to cover the electrolyte in the thin layer, and hence the temperature of the electrode, the plate employed to mount the cell onto the sample compartment of the spectrometer consisted of a hollow aluminium block fitted with inlet and outlet ports to allow the circulation of coolant from a Grant cooling/heating unit.^{22,23} The reflective working electrode was mounted on a Teflon body, and electrical contact was maintained by a screw and pushrod arrangement, which also maintained good optical contact between the working electrode and the cell window. The angle of incidence of the IR beam on the cell window was approximately 60° and the beam was directed to the detector via the electrode surface by the home built optical bench comprising four plane mirrors.

Each IR spectrum reported consisted of 64 summed and averaged scans with a resolution of 8 cm⁻¹ over ~ 16 s and are presented as (R/R_0) vs. wavenumber where R_0 is the reference spectrum and R is the spectra collected as a function of potential

or time. This data manipulation results in difference spectra in which positive peaks corresponding to $+(R/R_0)$ result from the loss of absorbing species in R with respect to R_0 and negative peaks corresponding to $-(R/R_0)$ to the gain of absorbing species.

The electrolyte solutions were prepared using Millipore water (18.2 MΩ cm) and analytical grade sulfuric acid (Aldrich). 0.1 M H₂SO₄ was employed as supporting electrolyte. Ethanol absolute CHRMASOLV (Aldrich) was used as received. 2 M Ethanol + 0.1 M H₂SO₄ solution was used in all measurements. Nitrogen gas from a cryogenic boil-off was employed to de-aerate the solutions and to maintain an air-free atmosphere over the electrolyte during the measurements. All potentials are given vs. Ag/AgCl reference electrode in saturated KCl solution.

The Pt (polycrystalline) electrode was “top hat” shaped with an area of 0.64 cm² and was polished before being exposed to the electrolyte. The electrode was polished using 0.3 and 0.015 μm alumina (BDH), washed thoroughly with Millipore water, and then immersed in Millipore water in an ultrasonic bath for 15 min prior to transfer into the spectro-electrochemical cell. The cleanliness of the electrode surface, electrolyte and cell were assessed by cyclic voltammetry.

The PtSn surface was prepared by the spontaneous deposition of Sn onto the Pt electrode from a solution of 0.01 M SnCl₂ + 0.1 M H₂SO₄ for 30 s. The surface Sn coverage was estimated to be ~0.30 using hydrogen adsorption/desorption charge in the cyclic voltammetry.^{12,13}

2.2 DFT Computational Methods

All the electronic structure calculations were performed using the Vienna Ab-initio Simulation Package (VASP) with Perdew-Burke-Ernzerh (PBE) generalized gradient approximation (GGA).²⁴⁻²⁶ The projector-augmented-wave (PAW) pseudopotentials were utilized to describe the core electron interaction²⁷ and the cut-off energy was 400 eV.

The calculation of phase diagram was based on the method reported by Rossmeisl *et al.*²⁸ Herein, a four-layer Pt(111) slabs, $p(4\times 4)$, was modelled with 64 atoms and a $3\times 3\times 1$ Monkhorst-Pack k -point sampling was used. Sn coverage was 0.0625 ML on Pt(111). A vacuum region of ~12 Å was placed between repeated slabs. In the calculations of reaction mechanisms, Pt(211) slabs were modelled by a 4-layer slab and a $p(3\times 4)$ supercell containing one (100) step was used with a $4\times 3\times 1$ Monkhorst-Pack k -point sampling. During all the optimizations, the top two layers and adsorbates were relaxed while the bottom two layers were fixed. All the transition states were localized with constrained minimization approach and the convergence of forces was set to 0.05 eV Å⁻¹.²⁹⁻³¹

Throughout the paper, blue denotes Pt atoms, grey denotes Sn atoms, white denotes hydrogen atoms, red denotes oxygen atoms and grey denotes carbon atoms.

3 Results and discussion

3.1 Electrochemistry of Pt and PtSn Surfaces in Acid Electrolyte

The surface electrochemistry and the EOR over a polycrystalline Pt electrode and the PtSn electrode were compared. Figure 1a shows the cyclic voltammetry (CV) measurements over the Pt and PtSn electrodes in a 0.1 M H₂SO₄ aqueous solution

supporting electrolyte. As expected, for the Sn modified surface, in the lower potential region, the hydrogen adsorption-desorption current was reduced due to the Pt sites being blocked by Sn adatoms. Approximately 1/3 of the total H-Pt sites were found to be blocked in agreement with the fact that Sn occupies 3-fold hollow sites on Pt.¹³ As each Sn atom blocks three H-Pt (on-top) sites, the Sn surface coverage is estimated to be ~0.30 which corresponds to ~0.10 monolayer (ML) with respect to surface Pt atom density. In addition, the CV shows that the typical double-layer region of pure Pt prior to surface OH(a) formation disappears on adsorption of Sn. Furthermore, the surface oxidation occurs at a much lower potential for the PtSn surface compared with Pt, 0.20 V and 0.45 V, respectively. This change in the surface oxidant formation potential is due to the ability of the surface to activate water and form OH(a). This is important in the activation of ethanol and ability of the catalyst to undertake further oxidation reactions.

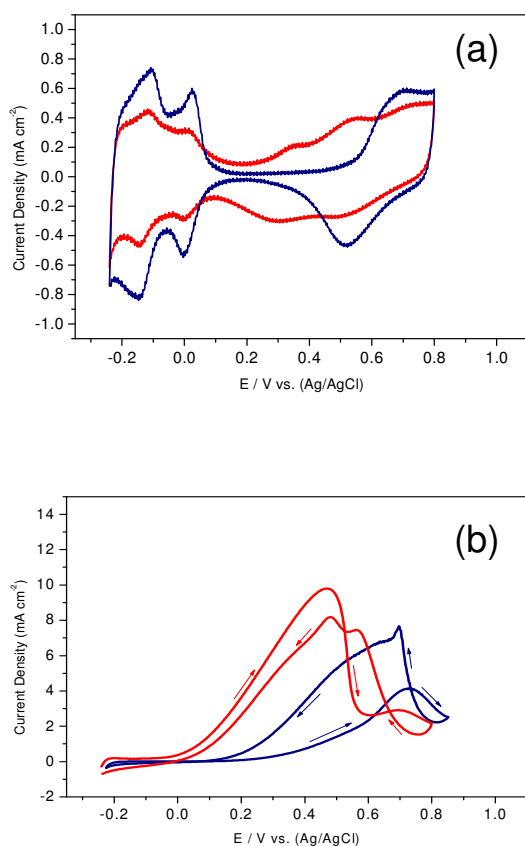


Fig.1 (a) Cyclic voltammograms of a clean polycrystalline Pt without (blue line) and with (red line) Sn adatoms in 0.1 M H₂SO₄ at 20 °C. (b) Cyclic voltammograms of the clean polycrystalline Pt without (blue line) and with (red line) Sn adatoms in 2M EtOH + 0.1M H₂SO₄ at 20 °C. In each case the scan rate was 0.200 V s⁻¹ and the coverage of Sn adatoms was estimated to be 0.30.

3.2 EOR at Pt and PtSn Electrodes

As expected, the CV on the PtSn electrode shows a significantly

higher activity for ethanol oxidation than that found for the pure Pt electrode (Figure 1b). The onset potential for the EOR in the forward potential scan shifts from around 0.30 V for Pt to around 0.00 V for the PtSn electrode, resulting in a marked increase in activity/current at all potentials up to 0.60 V. For example, at 0.40 V, the current density was approximately 20 times higher over the Sn modified surface compared with the pure Pt electrode. The lower activity found for the pure Pt electrode at potentials below 0.60 V is consistent with a low concentration of surface oxidants OH(a) as shown from the onset potential for surface oxidation in Figure 1a. At potentials above 0.60 V, surface oxidation occurs due to the formation of OH(a) oxidants and results in the increase in EOR current. Above 0.75 V, the EOR rate/current decreases due to the over oxidation of the platinum surface forming surface oxide which blocks ethanol adsorption and surface reaction.³² The PtSn surface facilitates the oxidant formation at a much lower potential (Figure 1a) which, in turn, promotes the EOR. As found for the pure Pt system, at too high a potential, in this case above 0.50 V, over oxidation occurs and a drop in EOR current is observed. For the pure Pt electrode, the forward scan results in much lower currents than the reverse scan. This is due to the presence of CO(a) formed from ethanol dissociation/dehydrogenation at lower potentials which results in the platinum surface being poisoned.^{33,34} On the reverse scan, the CO(a) has been removed by oxidation resulting in more surface site availability. In contrast, on the PtSn electrode the forward scan results in higher current than the reverse scan, indicating a reduced effect of CO(a) poisoning effect. This is consistent with the surface IR data presented in Figure 2.

Figures 2a-b and 2c-d show the *in-situ* FTIR spectra from Pt and PtSn electrocatalysts in 2 M ethanol + 0.1 M H₂SO₄ at 20 °C, respectively. The reference/background spectrum was collected at -0.20 V. Thereafter, the potential was increased to 1.10 V in the case of Pt and 0.80 V in the case of PtSn in 50 mV steps and IR spectra recorded at each step. The potential was limited to 0.80 V in the case of PtSn to avoid electrodisolution of the Sn. In Figure 2 only several representative spectra are shown for clarity.

From the spectra taken on pure Pt (Figures 2a-b), linearly bound CO adsorbates (CO_L)^{33,34} are observed at around 2055 cm⁻¹ from the dissociative adsorption/dehydrogenation of ethanol at ~0 V. With increasing potential up to 0.60 V, the CO_L IR band grew and, thereafter, it decreased with further increases in potential. At these potentials the growth of a band at 2340 cm⁻¹ associated with CO₂³³⁻³⁷ is observed which may indicate CO oxidation is occurring. In addition, at potentials above 0.35 V, a band at ~1716 cm⁻¹ is observed which grew significantly with increasing potential. This band is due to the C=O stretching in both acetaldehyde and acetic acid.^{33,34} Acetic acid also has a weak band at 1284 cm⁻¹ associated with coupling of the C-O stretching + OH deformation vibrations.^{33,34} This band is clearly visible at potentials above 0.60 V. These results show that ethanol is oxidized to acetaldehyde at potentials above 0.35 V, which in turn, is further oxidized to acetic acid at higher potentials (above 0.60 V) where the adsorbed acetate was also observed at ca. 1400 cm⁻¹.^{33,34} Table 1 summarizes the assignment of the FTIR bands for the intermediates and products of ethanol dissociative adsorption and oxidation reactions on the Pt electrode in sulphuric acid aqueous solution.

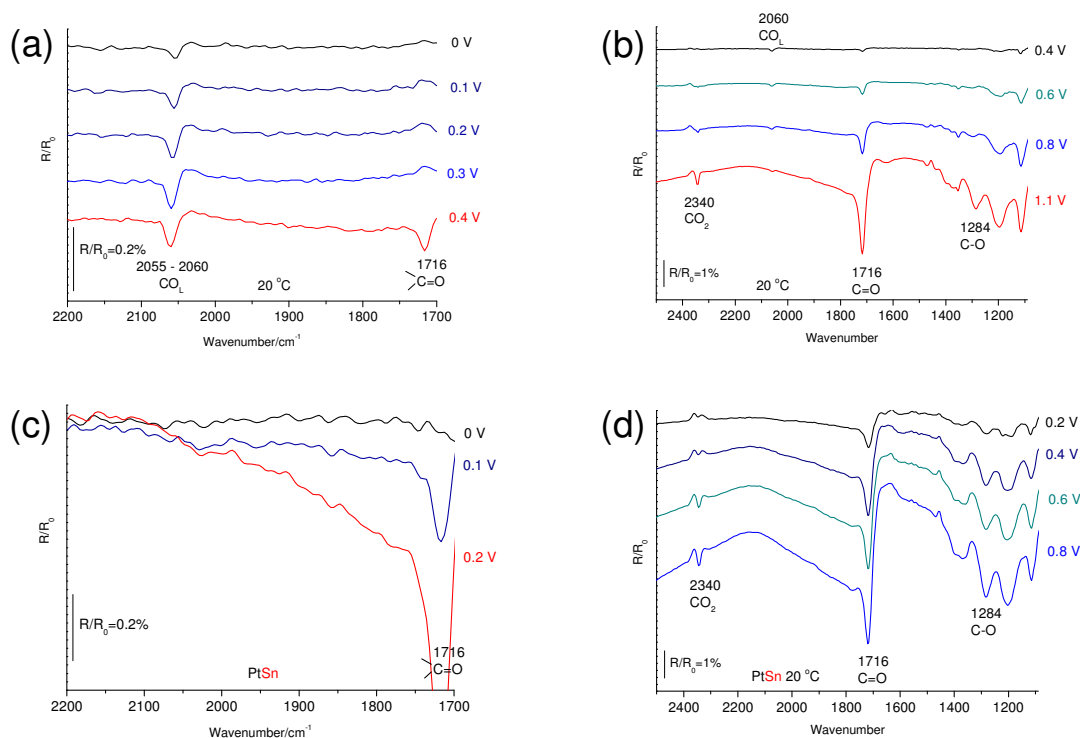


Fig. 2 *In-situ* FTIR spectra of the polycrystalline Pt without (a and b) and with (c and d) Sn adatoms in 2 M EtOH + 0.1 M H₂SO₄ at 20 °C. The spectra obtained with respect to a reference spectrum collected at -0.200 V. For clarity, only representative spectra are shown.

Table 1 Assignment of the FTIR bands observed during ethanol dissociative adsorption and oxidation on Pt and Sn-modified Pt electrodes.

| Band position/ cm ⁻¹ | Molecule/ functional group | IR mode |
|---------------------------------|-------------------------------|---|
| 2340 | CO ₂ | O=C=O asymmetric Stretching |
| 2050-2060 | CO _L | Linearly adsorbed CO |
| 1716 | -CHO or -COOH | C=O stretching |
| 1396-1420 | adsorbed -COO | O-C-O stretching of adsorbed acetate |
| 1284 | -COOH | Coupling C-O stretching + OH deformation |
| 1200 | HSO ₄ ⁻ | Asymmetric S-O stretching mode of bisulfate |

The *in-situ* FTIR data on the PtSn electrode (Figures 2c-d) show that the Sn modified surface inhibits the dissociative adsorption of ethanol to form CO_{ads} with only a very weak band observed at 2030 cm⁻¹ associated with CO_L at 20 °C. In contrast, it is clear that the PtSn surface facilitates ethanol oxidation to acetaldehyde and acetic acid with the growth of the band at *ca.*

1716 cm⁻¹ at an onset potential of 0.05 V. This is *ca.* 300 mV lower than found for the pure Pt surface. The amount of acetaldehyde and acetic acid formed on the PtSn surface was found to increase significantly on raising the potential, with the rate of change found to be much higher than that found over the pure Pt surface. The *in-situ* FTIR data agree with the CV data reported in Figure 1b and demonstrate that the changes observed in the currents are associated with the ability of the surface to promote C-C cleavage on ethanol adsorption and the subsequent effect of the surface CO inhibitor formed. Furthermore, it is also clear that, because the CO_{ads} formation route has been inhibited on the PtSn surface, the amount of CO₂ formed via CO_{ads} oxidation has been limited (Figures 2c-d).

Although fuel cells are normally operated at *ca.* 60 °C, to date, the majority of fuel cell electrocatalysis studies have only been performed at room temperature. This may be due to the aforementioned difficulty in engineering high temperature spectroelectrochemical cells. In this study, spectra were obtained at 60 °C using an in house designed variable temperature *in-situ* electrochemical FTIR system.^{22,23,35-37} The CV data (Figures S1-S3) show that with increasing temperature from 20 °C to 60 °C, the EOR is enhanced with the onset potential shifted by *ca.* 100 mV lower on both the pure Pt and PtSn electrodes. In addition, higher currents were observed compared with at 20 °C over a wider potential range above onset potential at *ca.* 0.3V.

At 60 °C, for the Pt surface (Figure S1), during the forward scan, there is a sharp increase in current above 0.30 V. This is in contrast with the slower increase in current observed at 20 °C, which indicates that there is a reduction in the inhibition of the surface due to CO adsorbates formed from ethanol dissociation.

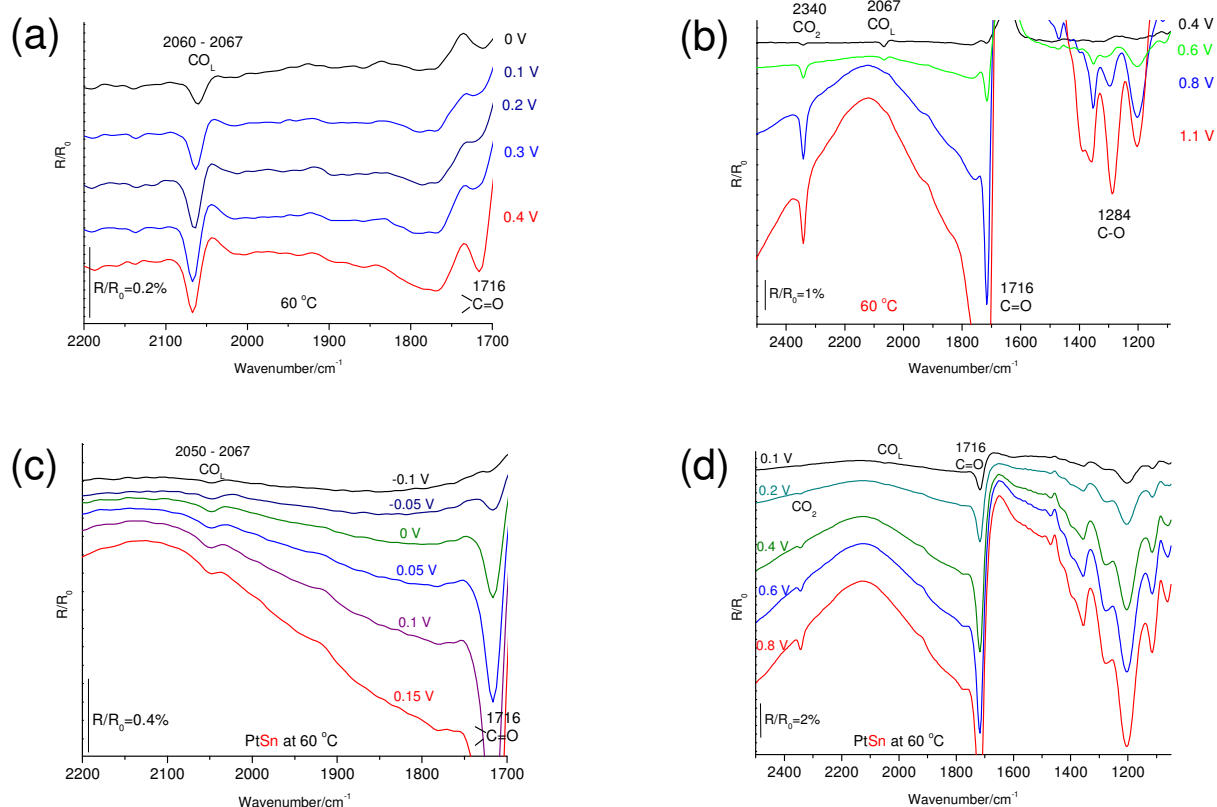


Fig. 3 *In-situ* FTIR spectra of the polycrystalline Pt without (a and b) and with (c and d) Sn adatoms in 2 M EtOH + 0.1 M H₂SO₄ at 60 °C. The spectra obtained with respect to a reference spectrum collected at -0.200 V. For clarity, only representative spectra are shown.

Furthermore, there is no excessive oxide blocking effect at potentials above 0.70 V as was observed at 20 °C. For the PtSn surface (Figure S2), at 60 °C, a lower onset potential \sim -0.075 V compared with \sim 0.00 V at 20 °C was observed, again with a significantly higher current. In this case, a small drop in current at potentials above 0.70 V was observed which may be compared with the larger related decrease found above 0.45 V at 20 °C. This was ascribed to surface oxide formation and shows that this effect is mitigated by the higher temperature. As found at 20 °C, the forward scan resulted in a higher current than that found for the reverse scan, which is consistent with the suggestion that little inhibition due to CO_{ads} occurs on the PtSn surface.

Figures 3a-b and 3c-d show the corresponding *in-situ* FTIR studies at 60 °C over the Pt and PtSn electrodes, respectively. For the Pt surface, comparing Figures 3a-b (60 °C) with Figures 2a-b (20 °C), it can be seen clearly that the higher temperature facilitates both ethanol dissociative adsorption to form CO_L adsorbates, shown by the presence of the band at \sim 2060 cm⁻¹ at lower potentials. CO_L electrooxidation to CO₂ was also observed, as shown by the growth in the band at \sim 2340 cm⁻¹ at potentials $>$ 0.30 V compared with that obtained at 0.50 V at 20 °C. In addition, the higher temperature significantly enhances the formation of acetaldehyde (1716 cm⁻¹) and acetic acid (1716 and 1284 cm⁻¹) at a lower onset potential of 0.25 V, at 60 °C, compared with 0.35 V, at 20 °C. As found at the lower temperature, acetate (1420 cm⁻¹) and bisulphate (1200 cm⁻¹,

formed from the supporting sulphuric acid electrolyte) were also observed at higher potentials.

Similarly, for the PtSn surface (Figures 2c-d compared with Figures 3c-d), increasing the temperature promotes ethanol oxidation to acetaldehyde (1716 cm⁻¹) and acetic acid (1716 and 1284 cm⁻¹) at lower onset potentials, -0.075 V (60 °C) vs. 0.025 V (20 °C). Interestingly, dissociative adsorption of ethanol to form CO_L is observed at 60 °C; this is in contrast with the absence of the process at 20 °C. The CO_L is then oxidized to CO₂ at potentials above 0.10 V. Whilst the Sn modification of the Pt does lead to the formation of CO adsorbate and subsequently CO₂ at 60 °C, oxidation of ethanol to acetaldehyde and acetic acid still dominates the overall EOR process. The strong IR band around 1200 cm⁻¹ observed is due to the bisulphate concentration increasing in the thin liquid electrolyte layer (between electrode surface and the IR window) probed in the IR and results from the consumption of water during the EOR (CH₃CH₂OH + H₂O \rightarrow CH₃COOH + 4H⁺ + 4e⁻).

3.3 DFT atomistic modelling

The rich and firsthand *in-situ* FTIR data above reveal clearly, at the molecular level, that Sn promotes ethanol oxidation to acetaldehyde and acetic acid, whilst inhibiting the ethanol dissociation to CO_{ads}. In order to explain these data and to gain a

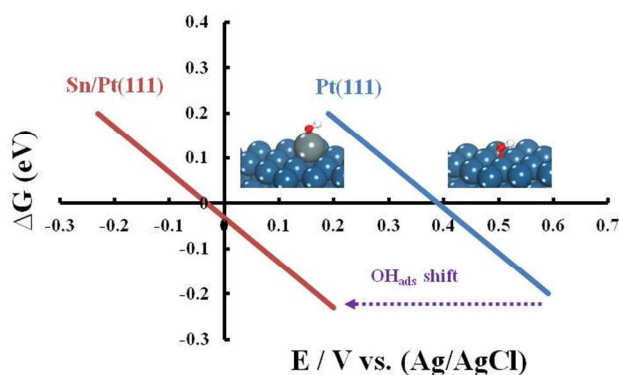


Fig. 4 Calculated phase diagram of OH adsorption on Pt(111) and Sn/Pt(111).

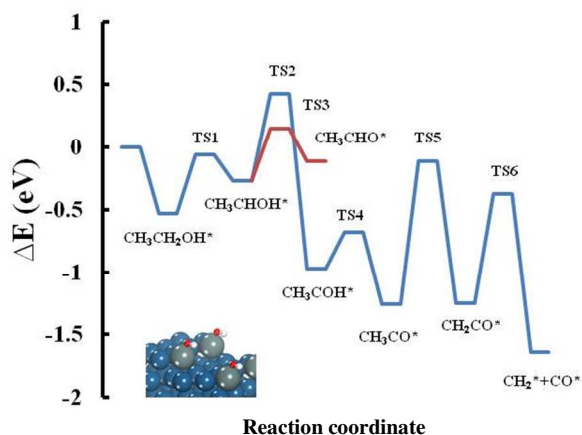


Fig. 5 Energy profiles of ethanol adsorption and electrooxidation on Sn/Pt(211). Red line indicates the formation of acetaldehyde and the blue line indicates the formation of CO. Insert corresponds to the initial surface structure.

deeper understanding of the Sn effects at the atomic and electronic levels, we have performed first-principles simulations using DFT calculations. We used flat Pt(111), stepped Pt(211) and the corresponding Sn modified surfaces to mimic the polycrystalline Pt and PtSn electrodes. It is well known that polycrystalline Pt surface consists mainly of flat (111) facets, together with some common defect sites such as the monatomic stepped (211) facets which have the (100) monatomic steps, separated by (111) terraces.³⁸ On pure platinum anode, the reaction is initiated by the formation of OH oxidant from water dissociation on the Pt sites; in our calculations, the onset potential of OH formation on Pt(111) is 0.39 V (vs. Ag/AgCl, pH = 1), which is consistent with the experimentally determined onset potential (around 0.30 V) in the electrooxidation of ethanol on pure Pt. In the phase diagram (Figure 4), it can be seen clearly that the Sn modified Pt(111) surface lowers the onset potential of OH formation from 0.39 V (on Pt sites) to -0.03 V (on PtSn sites), indicating that the modification of Pt by Sn can provide water dissociation (reaction (1)) sites at low potentials. It is worth mentioning that the OH adsorption energies were calculated on

both the Sn on Pt(111) and the Sn included in the lattice (a surface alloy with Pt), the difference between these two PtSn configurations is only 0.02 eV which is insignificant.



Interestingly, the addition of Sn on the Pt(211) surface (Figure S4) increases the onset potential for OH formation compared with the clean surface from -0.51 V (on Pt sites) to -0.29 V (on PtSn sites) due to defect site blocking, i.e., the step sites on pure Pt are more active for OH dissociation in water compared with the site when modified by Sn. However, in both cases the onset potential of OH oxidant formation on the (211) surface is lower than that found on the (111). As discussed above, the electrochemical and *in-situ* FTIR data show that the addition of Sn modifies both the rate and the selectivity to CO/CO₂ vs. acetaldehyde/acetic acid. To obtain a further insight into the reaction mechanisms at the electronic level, the energy profiles for ethanol adsorption and reaction over the (111) and (211) surfaces, with and without Sn, were examined in detail. The reaction profile for Pt(211) without and with Sn are shown in Figure S5 and Figure 5, respectively, with the corresponding optimised surface structures and transition states shown in Figure S6 and Figure 6, respectively. Table 2 summarises the activation barriers and reaction energies for each process over both Sn-modified and unmodified Pt(211) surfaces. It is clear from these data that, in the presence of Sn, the formation of acetaldehyde is more facile than pure Pt(211), as shown by the decrease in the barrier in the rate determining step for the formation of acetaldehyde (CH₃CHOH → CH₃CHO) on addition of Sn from 0.79 eV to 0.42 eV. In addition, the barriers for two of the steps which lead to CO and CO₂ increase on the addition of Sn. The barrier for the reactions of CH₃CO → CH₂CO and CH₂CO → CH₂ + CO increased from 0.97 eV to 1.15 eV and from 0.50 eV to 0.88 eV, respectively. These changes in the activation barriers on the addition of Sn to Pt are consistent with the experimentally observed decrease in CO/CO₂ selectivity on surface modification. In contrast, examining the energy barrier for the acetaldehyde formation on the Pt(111) surfaces with and without Sn modification for the ethanol partial oxidation reaction shows a decrease from 0.55 eV to 0.38 eV on the addition of Sn to the Pt (Table 3). On this surface C-C bond dissociation is unlikely to occur,³⁸⁻⁴⁰ even in the presence of Sn. Therefore, in the absence of Sn, although the barrier for C-C bond dissociation on the (211) surface is higher than that for the acetaldehyde formation on the (111) surface (0.97 eV vs. 0.55 eV), the significantly more facile OH formation on the stepped surface allows the two reactions to compete and both CO/CO₂ and acetaldehyde/acetic acid are formed. In contrast, in the presence of Sn, both the OH formation and C-C dissociation are more difficult on the stepped surface, whereas the acetic acid formation is more facile over both (211) and (111) surfaces, shifting the selectivity strongly towards acetic acid. The large increase in rate observed is therefore associated with both the decrease in the activation barriers as well as the increased concentration of surface OH at low potential on the (111) surfaces due to the presence of Sn. It is estimated from this data that, with addition of Sn, the rate of ethanol partial oxidation reaction is increased by two orders of magnitude at 25 °C.

Table 2 Calculated activation barriers (E_a) and reaction energies (ΔE) in eV for the reactions associated with the adsorption and electrooxidation of ethanol over pure Pt(211) and Sn modified Pt(211) at 25 °C.

| Surfaces | Pt(211) | | Sn/Pt(211) | |
|---|---------|------------|------------|------------|
| | E_a | ΔE | E_a | ΔE |
| Reactions | | | | |
| $\text{CH}_3\text{CH}_2\text{OH} \rightarrow \text{CH}_3\text{CH}_2\text{OH}^*$ | - | -0.47 | - | -0.53 |
| $\text{CH}_3\text{CH}_2\text{OH}^* \rightarrow \text{CH}_3\text{CHOH}^* + \text{H}^*$ | 0.61 | -0.32 | 0.46 | -0.27 |
| $\text{CH}_3\text{CHOH}^* \rightarrow \text{CH}_3\text{COH}^* + \text{H}^*$ | 0.63 | -0.63 | 0.70 | -0.70 |
| $\text{CH}_3\text{CHOH}^* \rightarrow \text{CH}_3\text{CHO}^* + \text{H}^*$ | 0.79 | 0.01 | 0.42 | 0.16 |
| $\text{CH}_3\text{COH}^* \rightarrow \text{CH}_3\text{CO}^* + \text{H}^*$ | 0.29 | -0.54 | 0.29 | -0.29 |
| $\text{CH}_3\text{CO}^* \rightarrow \text{CH}_2\text{CO}^* + \text{H}^*$ | 0.97 | 0.09 | 1.15 | 0.01 |
| $\text{CH}_2\text{CO}^* \rightarrow \text{CH}_2^* + \text{CO}^*$ | 0.50 | -0.76 | 0.88 | -0.40 |

Table 3 Calculated activation barriers (E_a) and reaction energies (ΔE) in eV for the reactions associated with the adsorption and electrooxidation of ethanol over pure Pt(111) and Sn modified Pt(111) at 25 °C.

| Surfaces | Pt(211) | | Sn/Pt(211) | |
|---|---------|------------|------------|------------|
| | E_a | ΔE | E_a | ΔE |
| Reactions | | | | |
| $\text{CH}_3\text{CH}_2\text{OH} \rightarrow \text{CH}_3\text{CH}_2\text{OH}^*$ | - | -0.28 | - | -0.34 |
| $\text{CH}_3\text{CH}_2\text{OH}^* \rightarrow \text{CH}_3\text{CHO}^* + 2\text{H}^*$ | 0.55 | 0.22 | 0.38 | -0.37 |

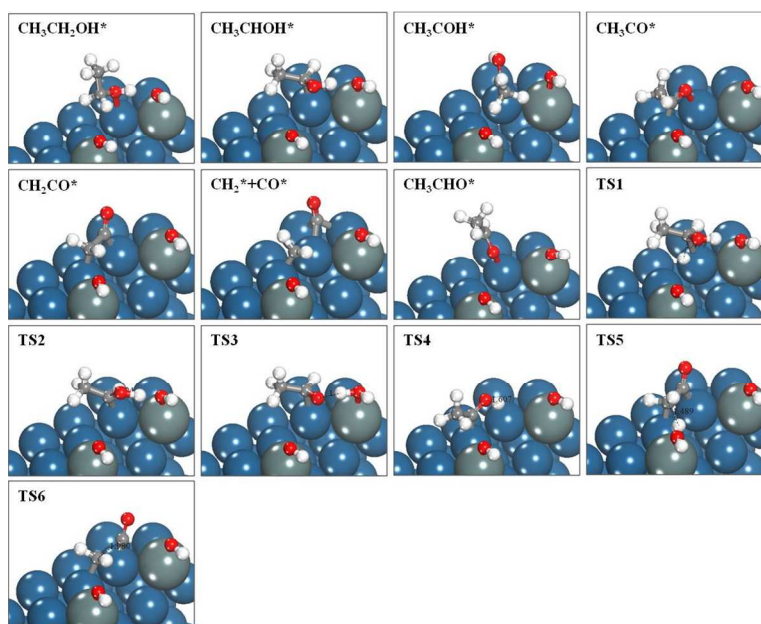


Fig. 6 Optimized structures and located transition states during the ethanol adsorption and electrooxidation on Sn/Pt(211). The transition states, denoted as TS, correspond to the points in the reaction profile shown in Figure 5.

It is worth pointing out that our DFT calculations are not only in good agreement with our firsthand electrochemical and *in-situ* FTIR data presented above, but also further explain the experimental data at the electronic level and reveal the complexity of the effects of the Sn on the Pt, with regards to both the surface reaction processes and the activity and selectivity issues in ethanol electro-oxidation over the most active PtSn catalysts.

In summary, taking all the data obtained from both stepped (211) and flat (111) surfaces, it is clear that whilst the activity of the Sn modified Pt surface towards ethanol oxidation reaction (EOR) increases, due to the higher surface concentration of OH(a) thanks to the lower onset potential for its formation on the (111) surface. The presence of OH and Sn promotes partial oxidation over C-C bond breaking leading to efficient acetaldehyde and acetic acid production over CO and CO₂ formation.

Overall, the results of the DFT modelling highlight the need for careful control of surface oxidant and its coverage that will allow facile ethanol adsorption and C-C bond cleavage whilst also providing sufficient levels and paths of CO oxidation. This is likely to be most successful through the use of mixed doping agents in addition to Sn.

4 Conclusions

By combining *in-situ* electrochemical FTIR data and DFT calculations, an insight into the ethanol fuel cell catalysis of the most active binary catalyst, PtSn, at the atomic and molecular levels, has been obtained for the first time. In comparison with pure Pt, the Sn modified Pt surface promotes active surface oxidant OH(a) formation with a lower onset potential. The Sn was found to increase the barrier for ethanol C-C bond breaking at the step edge on Pt(211) thus inhibiting the CO_{ads} formed at all the potentials studied. In contrast, the Sn facilitates ethanol dehydrogenation and partial oxidation to acetaldehyde and acetic acid as well as OH formation on Pt(111) leading to a higher rate of ethanol oxidation but lower selectivity to CO and CO₂ than for the unmodified system. Increasing the temperature from 20 °C to 60 °C facilitates both ethanol dissociation to CO_{ads} and oxidation to CO₂, resulting in an increased selectivity towards CO₂, but acetaldehyde and acetic acid are still the dominant products. This work reveals the complexity of catalytic reactions taking place at electrochemical interface and emphasises that for practical ethanol fuel cell applications, the most active PtSn catalysts still need to be improved in terms of selectivity towards total oxidation of ethanol to CO₂ to release the maximum 12 electrons per ethanol molecule.

Acknowledgments

This work was supported by the EPSRC (TS/H001875/1), Johnson Matthey plc. and the Technology Strategy Board. T.S. thanks the EPSRC (EP/I013229/1) for a research studentship, X.L. thanks QUB for the award of the title of Visiting Research Associate and P.H. thanks DEL for a studentship.

Notes and references

^a School of Chemistry and Chemical Engineering, Queen's University Belfast, Belfast BT9 5AG, UK.

⁶⁰ E-mail: c.hardacre@qub.ac.uk; w.lin@qub.ac.uk

^b Johnson Matthey Technology Centre, Blounts Court, Sonning Common, Reading RG4 9NH, UK

† Electronic Supplementary Information (ESI) available: [Cyclic voltammograms of Pt and PtSn electrodes in the presence of ethanol at 60 °C (Figures S1-3), phase diagram of OH adsorption on Pt(211) and Sn/Pt(211) (Figure S4), energy profiles of ethanol adsorption and electrooxidation on Pt(211) (Figure S5), optimized structures and located transition states during the ethanol adsorption and electrooxidation on Pt(211) (Figure S6)]. See DOI: 10.1039/b000000x/

- Z. G. Shao, F. Zhu, W. F. Lin, P. A. Christensen, H. Zhang, *Phys. Chem. Chem. Phys.*, 2006, **8**, 2720.
- Z. G. Shao, F. Zhu, W. F. Lin, P. A. Christensen, H. Zhang, *J. Power Sources*, 2006, **161**, 813.
- Z. G. Shao, W. F. Lin, P. A. Christensen, H. Zhang, *Int. J. Hydrogen Energy*, 2006, **31**, 1914.
- Z. G. Shao, F. Zhu, W. F. Lin, P. A. Christensen, H. Zhang, B. L. Yi, *J. Electrochem. Soc.*, 2006, **153**, A1575.
- N. Tian, Z. Y. Zhou, S. G. Sun, Y. Ding, L. W. Zhong, *Science*, 2007, **316**, 732.
- A. Kowal, M. Li, M. Shao, K. Sasaki, M. B. Vukmirovic, J. Zhang, N. S. Marinkovic, P. Liu, A. I. Frenkel, R. R. Adzic, *Nat. Mater.*, 2009, **8**, 325.
- M. Li, D. A. Cullen, K. Sasaki, N. S. Marinkovic, K. More, R. R. Adzic, *J. Am. Chem. Soc.*, 2013, **135**, 132.
- J. Melke, A. Schoekel, D. Dixon, C. Cremers, D. Ramaker, C. Roth, *J. Phys. Chem. C*, 2010, **114**, 5914.
- F. Vigier, C. Coutanceau, F. Hahn, E. M. Belgsir, C. Lamy, *J. Electroanal. Chem.* 2004, **563**, 81.
- C. Lamy, S. Rousseau, E. Belgsir, C. Coutanceau, J. Leger, *Electrochim. Acta*, 2004, **49**, 3901.
- F. Vigier, S. Rousseau, C. Coutanceau, J. Leger, C. Lamy, *Top. Catal.* 2006, **40**, 111.
- A. El-Shafei, M. Eiswirth, *Surf. Sci.* 2010, **604**, 862.
- Q. W. Zheng, C. J. Fan, C. H. Zhen, Z. Y. Zhou, S. G. Sun, *Electrochim. Acta*, 2008, **53**, 6081.
- A. V. Tripkovic, K. Popovic, J. Lovic, V. Jovanovic, S. Stevanovic, D. V. Tripkovic, A. Kowal, *Electrochem. Commun.*, 2009, **11**, 1030.
- L. Jiang, G. Q. Sun, S. G. Sun, J. G. Liu, S. H. Tang, H. Q. Li, B. Zhou, Q. Xin, *Electrochim. Acta*, 2005, **50**, 5384.
- M. Zhu, G. Q. Sun, Q. Xin, *Electrochim. Acta*, 2009, **54**, 1511.
- L. Jiang, L. Colmenares, Z. Jusys, G. Q. Sun, R. J. Behm, *Electrochim. Acta*, 2007, **53**, 377.
- Q. Wang, G. Q. Sun, L. Jiang, Q. Xin, S. G. Sun, Y. X. Jiang, S. P. Chen, Z. Jusys, R. J. Behm, *Phys. Chem. Chem. Phys.*, 2007, **9**, 2686.
- E. Antolini, E. R. Gonzalez, *Electrochim. Acta* 2010, **55**, 6485.
- F. Colmati, E. Antolini, E. R. Gonzalez, *J. Electrochem. Soc.*, 2007, **154**, B39;
- F. Colmati, E. Antolini, E. R. Gonzalez, *J. Solid State Electrochem.* 2008, **12**, 591.
- W. F. Lin, J. M. Jin, P. A. Christensen, F. Zhu, Z. G. Shao, *Chem. Eng. Comm.*, 2008, **195**, 147
- J. M. Jin, W.F. Lin, P. A. Christensen, *Phys. Chem. Chem. Phys.*, 2008, **10**, 3774.
- G. Kresse, J. Hafner, *Phys. Rev. B*, 1994, **49**, 14251.
- G. Kresse, J. Furthmuller, *Comput. Mater. Sci.* 1996, **6**, 15.
- J. P. Pedrew, K. Burke, M. Ernzerhof, *Phys. Rev. Lett.* 1996, **77**, 3865
- G. Kresse, D. Joubert, *Phys. Rev. B* 1999, **59**, 1758.
- J. Rossmeisl, J. K. Norskov, C. D. Taylor, M. J. Janik, M. Neurock, *J. Phys. Chem. B* 2006, **110**, 21833.
- A. Alavi, P. Hu, T. Deutsch, P. L. Silvestrelli, P. L.; J. Hutter, *Phys. Rev. Lett.* 1998, **80**, 3650.
- A. Michadelides, Z. P. Liu, C. J. Zhang, A. Alavi, D. A. King, P. Hu, *J. Am. Chem. Soc.* 2003, **125**, 3704.

- 31 Z. P. Liu, P. Hu, *J. Am. Chem. Soc.* 2003, **125**, 1958.
- 32 H. A. Gasteiger, N. Markovic, P. N.; Ross, E. J. Cairns, *J. Phys. Chem.* 1994, **98**, 617.
- 33 F. Colmati, G. Tremiliosi-Filho, E. R. Gonzalez, A. Berna, E. Herrero, J. M. Feliu, *Faraday Discuss.* 2008, **140**, 379.
- 5 34 X. H. Xia, H. D. Liess, T. Iwasita, *J. Electroanal. Chem.* 1997, **437**, 233.
- 35 W. F. Lin, M. S. Zei, M. Eiswirth, G. Ertl, T. Iwasita, W. Vielstich, *J. Phys. Chem. B* 1999, **103**, 6968.
- 10 36 H. X. Liu, N. Tian, M. P. Brandon, Z. Y. Zhou, J. L. Lin, C. Hardacre, W. F. Lin, S. G. Sun, *ACS Catalysis* 2012, **2**, 708.
- 37 P. A. Christensen, J. M. Jin, W. F. Lin, A. Hamnett, *J. Phys. Chem. B* 2004, **108**, 3391.
- 38 H. F. Wang, Z. P. Liu, *J. Am. Chem. Soc.*, 2008, **130**, 10996.
- 15 39 R. Kavanagh, X. M. Cao, W. F. Lin, C. Hardacre, P. Hu, *Angew. Chem. Int. Ed.*, 2012, **51**, 1572.
- 40 R. Kavanagh, X. M. Cao, W. F. Lin, C. Hardacre, P. Hu, *J. Phys. Chem. C*, 2012, **116**, 7185.

20